

Optimization of Draft Tube Structure for the Pilot-Scale Airlift Reactors

Luhaibo Zhao¹, Zhiyong Tang¹, Xiaojiao Luo¹, Wei Han¹, Min LV^{1*} and Yuhan Sun^{1,2*}

¹CAS Key Laboratory of Low-Carbon Conversion Science and Engineering, Shanghai 201210, China

²State Key Lab of Coal Conversion, Institute of Coal Chemistry, Chinese Academy of Science, Taiyuan 030001, China

Abstract

The effects of draft tube structure on the performance of pilot-scale Internal Loop Airlift Reactors (IL-ALRs) were investigated by Computational Fluid Dynamic (CFD) simulations and experiments. The Euler-Euler two fluid model and the κ - ϵ turbulence model were adopted in the CFD model to predict the influence of draft-tube structure on the key flow parameters including gas holdup, gas distribution and liquid circulation velocity. A good agreement was obtained between the CFD predictions and experimental measurements. In present study, perforation was applied to the expanding section of the draft tube, and numerical results show the optimized structure can enhance the gas-liquid separation, promote the oriented liquid circulation, increase the superficial gas velocity and maximize the productivity. Further optimization was conducted on the perforated design based on the CFD simulation.

Keywords: Pilot-scale airlift reactors; Draft-tube; Multiphase fluid; CFD simulation

Nomenclature: $G_{1\epsilon}, G_{2\epsilon}, G_{\mu}$: Turbulence model coefficient; G_{κ}, G_b : Turbulent kinetic energy; \vec{F}_k : Interphase forces, $\text{N}\cdot\text{m}^{-3}$; \vec{F}_d : Drag force, $\text{N}\cdot\text{m}^{-3}$; \vec{F}_{vm} : Virtual mass force, $\text{N}\cdot\text{m}^{-3}$; \vec{F}_{lift} : Lift force, $\text{N}\cdot\text{m}^{-3}$; H: Liquid level, m; Hd: Sealed downcomer height; Dd: Sealed downcomer diameter; He: Expanded downcomer height; De: Expanded downcomer diameter; Hp: Perforated downcomer height; s, s : Unit matrix; S_{κ}, S_{ϵ} : User-defined source terms; U_g : Superficial gas velocity, $\text{m}\cdot\text{s}^{-1}$; \vec{v}_k : The k phase velocity vector, $\text{m}\cdot\text{s}^{-1}$; Y_M : The contribution of the fluctuating dilatation in compressible turbulence to the overall dissipation rate; C_D, C_v, C_l : Interphase forces coefficient; Re: Reynolds number; g: Gravitational acceleration, $\text{m}\cdot\text{s}^{-2}$; p: Pressure, Pa; t: Time, s; k1: Gas phase; k2: Liquid phase; α_k : The kth phase volume fraction; E: Turbulent dissipation rate, $\text{m}^2\cdot\text{s}^{-3}$; κ : Turbulent kinetic energy, $\text{m}^2\cdot\text{s}^{-2}$; ρ_k : The kth phase density, $\text{kg}\cdot\text{m}^{-3}$; $\vec{\tau}_k$: The stress-strain tensor, $\text{N}\cdot\text{m}^{-2}$; μ_k : The shear viscosity, Pa·s; λ_k : The bulk viscosity, Pa·s; μ_t : The turbulent viscosity, Pa·s; $\sigma_{\kappa}, \sigma_{\epsilon}$: Turbulent Prandtl numbers; d_b : Bubble diameter, mm

Introduction

Airlift Reactor (ALR) has been widely applied in the chemical and petrochemical industries (such as FT process, methanol synthesis), biochemical fermentation (microalgae cultivate), as well as wastewater treatment. It has a relative simple mechanical structure without internal or moving parts, which is easy to scale up, low shear stress, excellent heat and mass transfer efficiency, and good mixing characteristics with low energy consumption. The design of ALRs is based on the Bubble Columns (BCs) and the addition of internal airlift loop could enhance the oriented fluids circulation and reduce the irregular flows. Therefore, for the three-phase system with the present solid catalyst, it can improve the liquid-catalyst slurry circulation, hence avoid the accumulation of the catalyst, prevent the hotspot which causing deactivation of the catalyst, and ultimately increase the space-time yield [1-3].

In general, the airlift reactors are classified into two categories: External Loop Airlift Reactors (EL-ALRs) and Internal Loop Airlift Reactors (IL-ALRs). The former is composed of two conduits connected at the top and the bottom, while the latter consists of two concentric cylinders [4]. A typical internal loop airlift reactor mainly consists of four sections named as riser, draft tube, top and bottom section. The density difference induced by the gas holdup difference between the riser and draft tube is the main driving force for the liquid circulation in airlift reactors [5]. Gas holdup, liquid circulation velocity, bubble

size, bubble distribution and mass/heat transfer coefficient are the key hydrodynamic parameters for ALRs, a good understanding of the influence of operating conditions (superficial gas velocity, pressure etc.), reactor geometry, structures of gas sparger and internals on these parameters is essential for the design and scale-up of ALRs. Extensive studies on the hydrodynamics in the airlift reactors have been reported in the last decades [6-9] and most of the work has been focused on the design of reactor structure and gas sparger [10-13]. Though some of the work has been reported on the optimization of the diameter and expansion angle of the straight/expanded draft tubes [14], very few work has been carried out to systematically study the influence of draft tube on the flexibility of operation, the gas liquid mixing/separation and the heat/mass transfer. However, there are several problems about the ALRs with conventional sealed straight draft tube. For example, it is difficult to control the liquid level and circulation when the superficial gas velocity is too small or large. Therefore, in the present research, the work has been conducted to investigate three types of draft tubes: conventional sealed straight draft tube (Type A), conventional straight draft tube with expand section (Type B), and novel designed sectional perforated draft tube (Type C). A cold model facility was built up to exam the performance of various draft tubes, in the meantime, CFD simulations were performed to validate the experimental observations, as well as the design of the sectional perforated draft tube was further optimized.

Experimental Setup and Methods

The schematic diagram of the experimental facility is illustrated in Figure 1a. The pilot-scale airlift reactor consists of a Plexiglas column with the height of 3000 mm and internal diameter of 1200 mm and the reactor internals which mainly include a gas distributor and a

*Corresponding author: Yuhan Sun, CAS Key Laboratory of Low-Carbon Conversion Science and Engineering, Shanghai 201210, PR China, Tel: +86-21-203-250-09; E-mail: sunyh@sari.ac.cn

Min LV, CAS Key Laboratory of Low-Carbon Conversion Science and Engineering, Shanghai 201210, PR China, Tel: +86-21-203-509-57; E-mail: lvmin@sari.ac.cn

Received June 22, 2015; Accepted June 29, 2015; Published July 06, 2015

Citation: Zhao L, Tang Z, Luo X, Han W, Min LV, et al. (2015) Optimization of Draft Tube Structure for the Pilot-Scale Airlift Reactors. J Adv Chem Eng 5: 126. doi:10.4172/2090-4568.1000126

Copyright: © 2015 Zhao L, et al. This is an open-access article distributed under the terms of the Creative Commons Attribution License, which permits unrestricted use, distribution, and reproduction in any medium, provided the original author and source are credited.

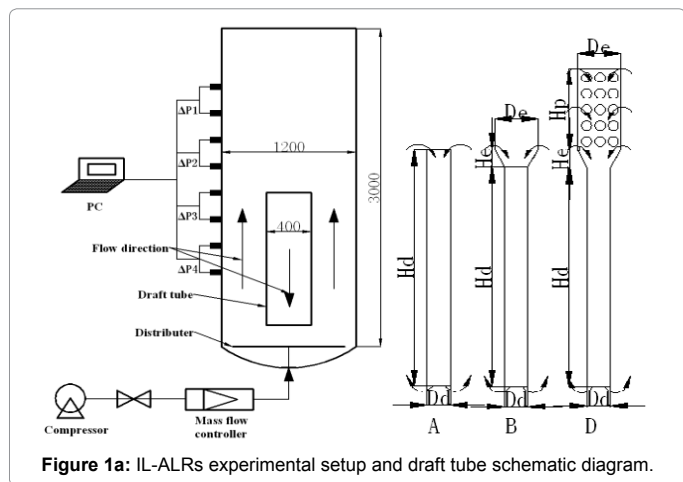


Figure 1a: IL-ALRs experimental setup and draft tube schematic diagram.

draft tube. The draft tube is placed in the center of the column and 100 mm above the gas sparger. The properties of three types of draft tube are determined empirically and summarized in Tables 1 and 2. The air was injected into the reactor through a ring sparger located at the bottom of the annulus section which is between the draft tube and the reactor column. Here, the bubbling experiment can be seen in Figure 1b. The annulus section and the draft tube served as the riser and the downcomer, respectively. The range of the superficial gas velocity was between 0.1 m/s to 0.5 m/s, similar to the industrial conditions. The liquid phase is mainly the tap water. The unaerated liquid level was 1200 mm, holding the top clearance of about 200 mm between the liquid surface and the upper end of the draft tube. The experimental instrumentations used in present study mainly include high speed photography, differential pressure transducer and conductivity probe. All the experiments were carried out at room temperature and atmospheric pressure.

Numerical simulations

The Euler-Euler two fluids model is applied in the CFD simulation. In this model, each phase is considered as a single fluid, hence the momentum and continuity equations are solved for each phase. And both gas and liquid phase were assumed as incompressible. The mathematical equations applied in this model are described as following:

The continuity equation for phase k is:

$$\frac{\partial}{\partial t}(\alpha_k \rho_k) + \nabla \cdot (\alpha_k \rho_k \vec{v}_k) = 0 \quad (1)$$

Where α_k , ρ_k , \vec{v}_k is the volume fraction, velocity, and density of phase k, respectively.

The momentum balance for phase k yields

$$\frac{\partial}{\partial t}(\alpha_k \rho_k \vec{v}_k) + \nabla \cdot (\alpha_k \rho_k \vec{v}_k \vec{v}_k) = -\alpha_k \nabla p - \nabla \cdot \bar{\tau}_k + \alpha_k \rho_k \vec{g} + \vec{F}_k \quad (2)$$

Where $\bar{\tau}_k$ is the kth phase stress-strain tensor. According to the Boussinesq hypothesis, the flow is described as isotropic turbulence.

$$\bar{\tau}_k = \alpha_k \mu_k (\nabla \vec{v}_k + \nabla \vec{v}_k^T) + \alpha_k (\lambda_k - \frac{2}{3}) \nabla \cdot \vec{v}_k \bar{I} \quad (3)$$

Where μ_k and λ_k are the shear and bulk viscosity of phase k, \bar{I} is unit matrix. Respectively, \vec{g} , p , \vec{F}_k are gravitational acceleration, pressure and inter-phase forces including a drag force \vec{F}_d , a virtual mass force \vec{F}_m and a lift force \vec{F}_{lift} .

$$\vec{F}_k = \vec{F}_d + \vec{F}_m + \vec{F}_{lift} \quad (4)$$

$$\vec{F}_d = \frac{3}{4} \alpha_{k1} \alpha_{k2} \frac{\rho_{k2}}{d_b} C_D |\vec{v}_{k1} - \vec{v}_{k2}| (\vec{v}_{k1} - \vec{v}_{k2}) \quad (5)$$

$$\vec{F}_m = C_v \alpha_{k1} \rho_{k2} \left(\frac{D\vec{v}_{k1}}{Dt} - \frac{D\vec{v}_{k2}}{Dt} \right) \quad (6)$$

$$\vec{F}_{lift} = C_l \alpha_{k1} \rho_{k2} (\vec{v}_{k1} - \vec{v}_{k2}) \times (\nabla \times \vec{v}_{k2}) \quad (7)$$

k1 is the gas phase and k2 is the liquid phase. The values of the interaction force parameters are listed in

Table 3.

$$Re = \frac{\rho_{k2} |\vec{v}_{k1} - \vec{v}_{k2}| d_b}{\mu_{k2}} \quad (8)$$

d_b is the bubble diameter. The bubble is assumed to be spherical without coalescence and breakage interaction, the mean diameter of which is about 8mm according to the experimental observations by using high speed camera and image processing software.

The standard κ - ϵ turbulence model is used to consider the turbulence of the multiphase flow in the IL-ALR. The flow is assumed to be fully turbulent, and the effects of molecular viscosity are negligible. The κ and ϵ equations describing this model are as follows:

$$\begin{aligned} \frac{\partial}{\partial t}(\kappa \rho_k) + \nabla \cdot (\kappa \rho_k U_k) &= \nabla \cdot \left[\left(\mu + \frac{\mu_t}{\sigma_\kappa} \right) \nabla \kappa \right] \\ + G_\kappa + G_b - \epsilon \rho_k - Y_M + S_\kappa \end{aligned} \quad (9)$$

Type	H_d	D_d	H_e	D_e	H_p
A-Straight	1250	400	0	0	0
B-Expanded	1050	400	200	630	0
C-Perforated	1050	400	200	630	750

Table 1: Parameters for three types of draft tube (mm).

Type	Percentage open area	Hole size (mm)	Number
C1	50%	10	38
C2	50%	30	13
C3	50%	50	8
C4	10%	10	8
C5	30%	10	22
C6	60%	10	45

Table 2: Parameters for orifices of type-C.

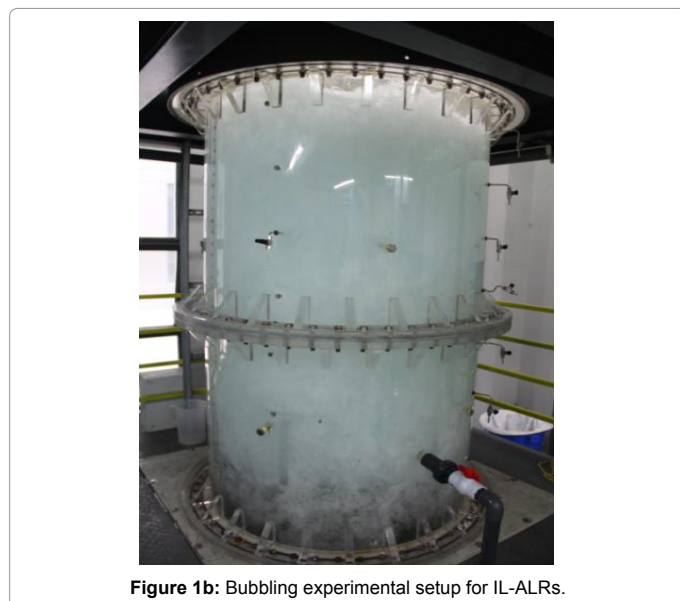


Figure 1b: Bubbling experimental setup for IL-ALRs.

C_b	C_v	C_i
$\begin{cases} 24(1+0.15Re^{0.687})/Re, Re \leq 1000 \\ 0.44, Re \geq 1000 \end{cases}$	0.5	0

Table 3: Parameters of interaction force between phases model.

$$\frac{\partial}{\partial t}(\varepsilon \rho_k) + \nabla \cdot (\varepsilon \rho_k U_k) = \nabla \cdot \left[\left(\mu + \frac{\mu_{t,k}}{\sigma_\varepsilon} \right) \nabla \varepsilon \right] + G_{1\varepsilon} \frac{\varepsilon}{K} (G_K + G_{3\varepsilon} G_b) - G_{2\varepsilon} \rho_k \frac{\varepsilon^2}{K} + S_\varepsilon \quad (10)$$

In these equations, G_K represents the generation of turbulence kinetic energy due to the mean velocity gradients. G_b is the generation of turbulence kinetic energy due to buoyancy. Y_M represents the contribution of the fluctuating dilatation in compressible turbulence to the overall dissipation rate. S_K and S_ε are user-defined source terms. The turbulent (or eddy) viscosity μ_t , is computed by combining κ and ε equations as follows:

$$\mu_t = \frac{C_\mu \rho_k \kappa^2}{\varepsilon} \quad (11)$$

The model constants have the following values shown in Table 4.

The model described above was implemented into the commercial CFD code ANSYS-Fluent with the pressure-based solver and transient simulation. The 2D model is used to study the effects of draft tube on the cylindrical internal loop airlift reactor. A second order spatially accurate QUICK scheme was employed to discrete all the equations. A multiphase variant of SIMPLE algorithm was implemented for pressure-velocity coupling. First order implicit time stepping was used to advance the solution in time. In all simulations, quasi-steady numerical solutions were obtained. The term “quasi-steady” means here that all variables at the end of calculations exhibited small oscillations around steady state values and statistical average was reached for all variables. The boundary conditions mainly included the gas velocity-inlet and the pressure-outlet. Non-slip boundary condition was assumed for the wall condition. Each simulation was running for 50 s, in the first 10 s, the time step is 0.005 s, then it reduce to 0.025 s for the rest of 40 s.

Grid independence test

For the numerical calculation, the accuracy, precision and speed depend on the quality of grid, so it is important to perform a grid independence test to decide an appropriate grid size, and the grid sizes studied are summarized in Table 5. Figure 2 is the numerical predictions for the radial distribution of time-averaged gas holdup at $H=0.75$ m, with three different levels of grid size. An identical result was obtained regardless of the grid refinement, indicating the level 1 grid size is sufficient for the simulation.

Result and Discussion

Effect of the draft-tube structure for total gas holdup and gas distribution

Figures 3 and 4 indicate the total gas holdup increased with the increasing superficial gas velocity, and it is in line with the measurement. More importantly, the results also indicated that the structure of the draft tube has certain influences on the gas holdup and gas distribution. The expanded section of type B draft tube leads to a reduction in the total gas holdup comparing with Type A, and this was further enhanced by the results from the perforated expansion section in Type C draft tube. Figure 4 indicates the improvements of the draft tube structure

could strengthen the gas-liquid separation, which leads to a more even distribution of the gas phase in the riser area, and prevent the slug flow in the downcomer area.

Effect of the draft-tube structure for local gas holdup

Figure 5 illustrates that the local gas holdup increases with the increasing gas superficial velocity in both riser and downcomer area, here, the measured location is from the bottom of the tube ($h=0.2$ m) to the liquid level. Furthermore, the influence of draft tube structure on the gas holdup in the riser area is negligible, but significant in the region of downcomer. With type A, large amount of gas was entrained into the bulk liquid that flows into the draft tube from the top, causing a higher gas holdup in the downcomer which could inhibit the flow circulation.

The expanded section of type B enhance the gas liquid separation at the top of draft tube, hence reduce the local gas hold up inside

$G_{1\varepsilon}$	$G_{2\varepsilon}$	G_μ	σ_κ	σ_ε
1.44	1.92	0.09	1.0	1.3

Table 4: Parameters of κ - ε model.

Grid level	1	2	3
cells	8585	16298	34135
nodes	9150	17072	35294

Table 5: Grid generation levels of the reactor.

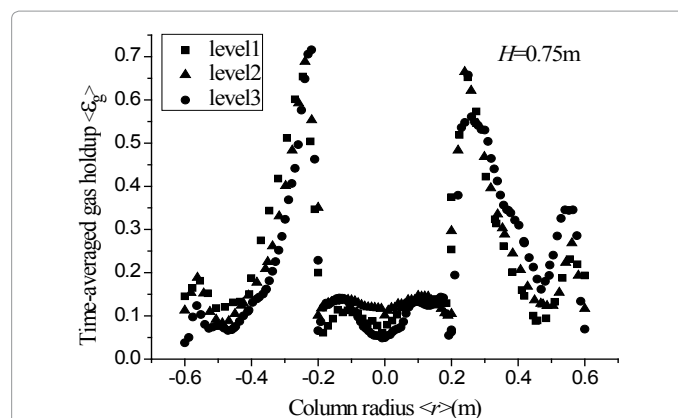


Figure 2: Radial distribution of time-averaged gas holdup at $H=0.75$ m (Type A, $U_g=0.3$ m/s).

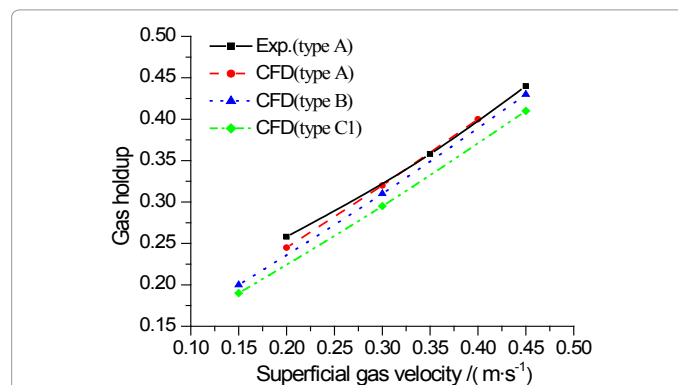


Figure 3: Effect of the draft-tube structure for total gas holdup with superficial gas velocity.

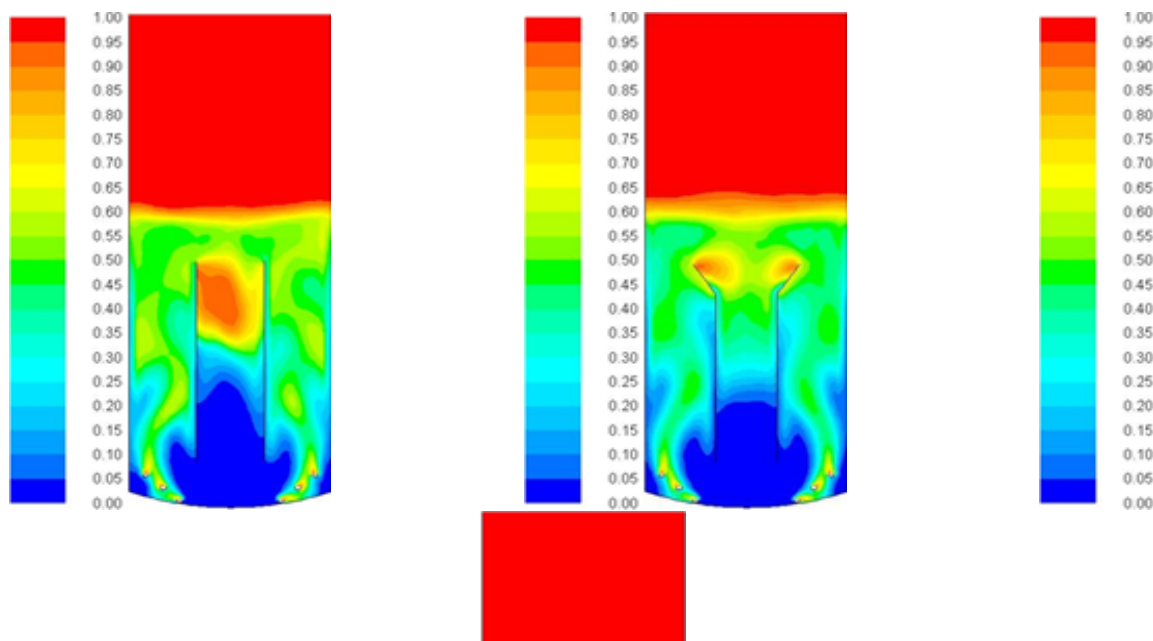


Figure 4: Time averaged gas volume fraction distribution ($U_g=0.3\text{m/s}$).

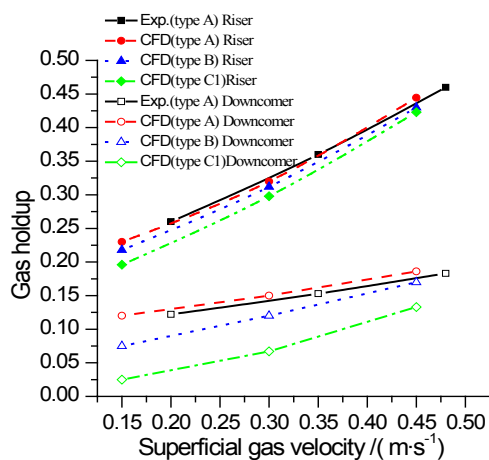


Figure 5: Time-averaged local gas holdup in the riser and down comer from bottom to the liquid level with superficial gas velocity.

the draft tube and improve the liquid circulation. However, the gas liquid separation is difficult for the higher gas velocity as the local gas holdup tends to be similar between type A and B. Therefore, Type C was designed in the present work to further enhance the gas liquid separation. As show in Figure 5, a lower gas holdup was obtained with Type C design for the entire range of gas velocities. .

Effect of the draft-tube structure for liquid circulation velocity

The liquid circulation velocity was also investigated by both experiment and CFD simulations and the results are shown in Figure 6. When the gas velocity is less than 0.3 m/s, the liquid circulation velocity is increased with the increasing gas velocity. Because the gas entrainment inside the draft tube is negligible in the lower range of gas velocity, the density difference between the inside and outside

of draft tube is increasing with increased gas velocity, and so does liquid circulation driving force. In addition, the circulation velocity is enhanced by Type B and C compare to Type A. However, different trends were observed when gas velocity exceeds 0.3 m/s. The liquid circulation velocities decreased with higher gas velocity for Type A and B, whereas the liquid circulation velocity kept increase with Type C draft tube. This is in agreement with the results in Figure 5. Above the critical gas velocity, in this case, 0.3 m/s, more gas was entrained in the liquid inside the draft tube of Type A and B, due to the lack of efficient gas liquid separation at the top of the draft tube. As a result, the liquid circulation was inhibited, causing lower circulation velocity. In contrast, a good gas liquid separation was achieved with Type C, as a result, an increasing trend of liquid circulation velocity was observed.

To summarize, the perforated expanding section structure applied in Type C was proved to be able to maximize the gas liquid separation, and enhance the axial liquid circulation. Particularly, it is more suitable than the traditional draft tube for the industrial scale reactors with the higher gas flux.

Effect of the hole diameter for gas holdup and liquid circulation velocity

As mentioned above, the perforation property of the expanding section in Type C is able to enhance the gas liquid separation. Therefore it is important to optimize the design of the perforation diameter, as well as the percentage open area. Figure 7 shows the influence of the perforation diameter on the local gas holdup. For a fixed percentage open area of 50%, the gas holdup inside and outside of the draft tube increase with the increasing perforation diameter. Particularly for the downcomer area, the larger hole size leads to a higher gas entrainment rate and consequently higher gas holdup.

Figure 8 shows that the perforation diameter has very little effect on the liquid circulation velocity in the range of lower gas velocity, $U_g < 0.3\text{m/s}$. However, further increasing the gas velocity, the advantage

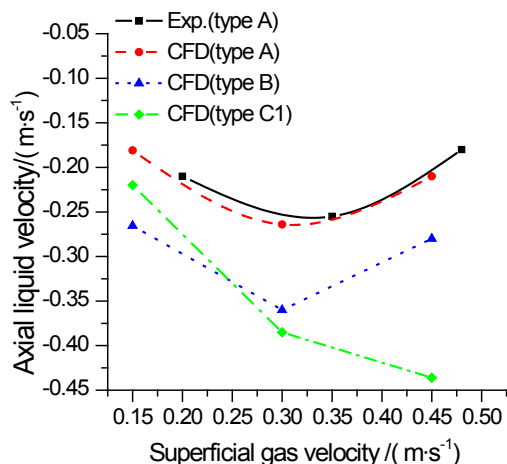


Figure 6: Axial liquid velocity in the downcomer with superficial gas velocity (minus present downward flow direction).

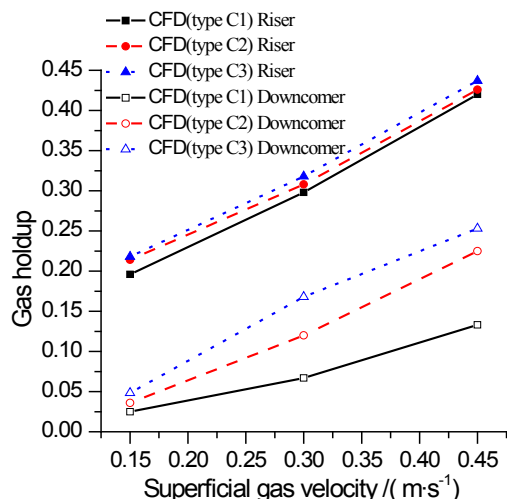


Figure 7: Time-averaged local gas holdup in the riser and downcomer from bottom to the liquid level with superficial gas velocity.

of the smaller hole size become more obvious since it can significant enhance the liquid circulation velocity, hence maximize the mass transfer efficiency.

Effect of the percentage open area for gas holdup and liquid circulation velocity

Optimizations of percentage open area for Type C draft tube were also performed and the corresponding results are shown in Figure 9. For a fixed perforation diameter of 10 mm, the decrease in the percentage open area leads to a higher gas holdup in the riser whereas a lower gas holdup in the downcomer. In the region of the riser, the lower percentage open area tends to constrain the gas-liquid flow upward, consequently leads to a higher gas holdup. At the top section of the downcomer, the lower percentage open area can achieve a better gas-liquid separation and the less gas content in the liquid.

Moreover, the effects of the percentage open area on liquid circulation velocity are also given in Figure 10. For the minimum percentage open area of 10%, a low axial liquid velocity in the downcomer is observed because the fluids are mainly blocked in the riser, which hardly flow into the draft tube. The increase of the percentage open

area could improve the liquid circulation velocity, but the trend is non-monotonic. In the range of lower superficial gas velocity, the liquid velocity increases with the increasing percentage open area because more fluids flow into the draft tube. However, above the critical gas velocity of 0.3 m/s, the efficiency of gas liquid separation becomes more significant. Therefore, the determination of the percentage open area should consider the amount of the fluids which flow into the draft tube, as well as the effectiveness of the gas-liquid separation. In this case, the optimized percentage open area is 50%.

Conclusion

The experimental and numerical investigations of the draft tube for the pilot scale airlift reactors were carried out in this research. A good agreement was obtained between the measurements and CFD simulation results. The structure of draft tube has significant influence on the multiphase flow dynamics in the IL-ALRs. Compare to the simplest structure of draft tube (Type A), both type B and C could improve the gas liquid separation, hence reduce the gas holdup in the downcomer and promote the liquid circulation. However, Type C

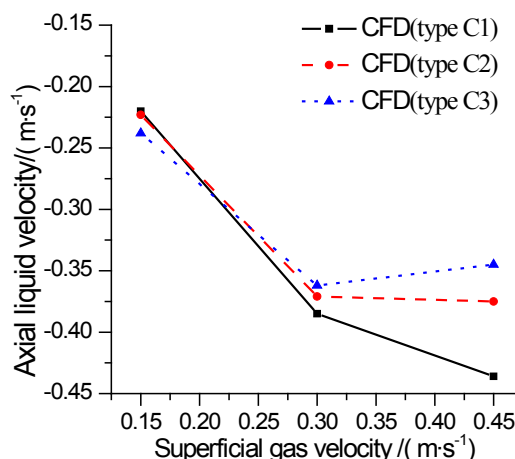


Figure 8: Axial liquid velocity in the downcomer with superficial gas velocity (minus present downward flow direction).

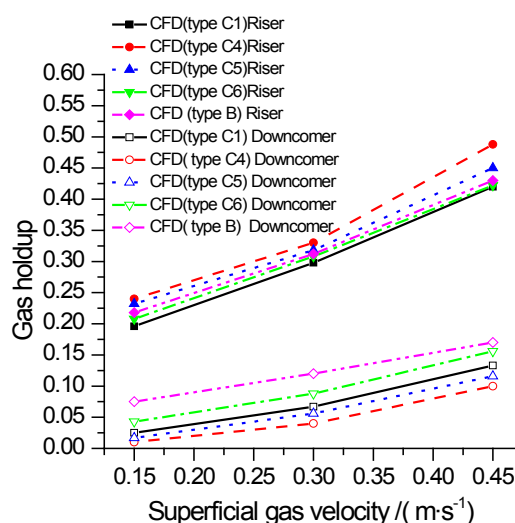


Figure 9: Time-averaged local gas holdup in the riser and downcomer from bottom to the liquid level with superficial gas velocity.

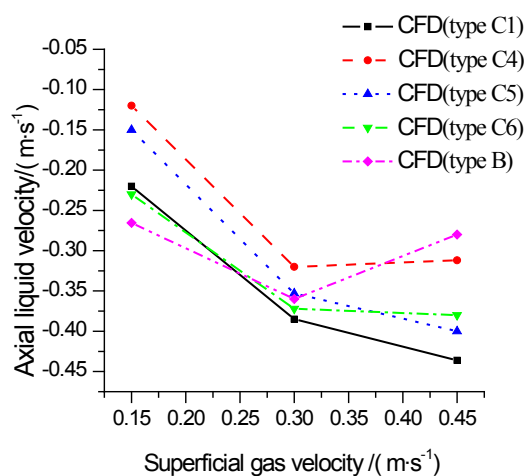


Figure 10: Axial liquid velocity in the downcomer with superficial gas velocity (minus present downward flow direction).

is more applicable for a wider range of the operational gas velocity, particularly for high gas velocity and space-time yield, it can further enhance the gas-liquid separation due to the additional perforation applied to the expanding section.

Optimization was carried out on the perforation structure of Type C draft tube in terms of perforation size and percentage open area. The perforation size has to be kept as small as possible, in this case, the smallest perforation size of 10mm was found most suitable. An increase in the perforation size allows more gas components penetrate into the downcomer, reduce the density difference between the downcomer and riser, and consequently restrain the liquid circulation. The choice of the percentage open area is more complicated. An increase in the percentage open area allows more fluids flow into the downcomer; hence increase the liquid circulation velocity, however, above a critical value, further increase the percentage open area would inhibit the gas liquid separation which is not desirable. The optimized percentage open area is 50%. The optimization of draft tube structure for the pilot-scale airlift reactors has a significant effect on design and scale-up of the ALRs, promoting the yield and reducing the energy consumption.

Acknowledgement

This project is jointly funded by BP, CECC and Lu'an group. The authors are grateful for their contribution, without their support the work would not have been possible.

References

1. Chisti MY (1989) Airlift Bioreactors. Elsevier Applied Science, London and New York.
2. Luo HP, Al-Dahhan MH (2008) Local characteristics of hydrodynamics in draft tube airlift bioreactor. Chem Eng Sci 63: 3057-3068.
3. Jin B, Yin P, Lant P (2006) Hydrodynamics and mass transfer coefficient in three phase air-lift reactors containing activated sludge. Chem Eng Proc 45: 608-617.
4. Baten JM, Ellenberger J, Krishna R (2003) Hydrodynamics of internal air-lift reactors: experiments versus CFD simulations. Chem Eng Proc 42: 733-742.
5. Xu YY, Luo LJ, Yuan JQ (2011) CFD Simulations to portray the bubble distribution and the hydrodynamics in an annulus sparged air-lift bioreactor. Can J Chem Eng 89: 360-368.
6. Chisti MY, Hallard B, Moo-Young M (1988) Liquid circulation in airlift reactors. Chem Eng Sci 43: 451-457.
7. Kilonzo PM, Margaritis A, Bergougnou MA (2010) Hydrodynamics and mass transfer characteristics in an inverse internal loop airlift-driven fibrous-bed bioreactor. Chem Eng J 157: 146-160.
8. Blazej M, Kisa M, Markos J (2004) Scale influence on the hydrodynamics of an internal loop airlift reactor. Chem Eng Proc 43: 1519-1527.
9. Olivieri G, Marzocchella A, Ommen JR, Salatino P (2007) Local and global hydrodynamics in a two-phase internal loop airlift. Chem Eng Sci 62: 7068-7077.
10. Lu XP, Ding J, Wang YR, Shi J (2000) Comparison of the hydrodynamics and mass transfer characteristics of a modified square airlift reactor with common airlift reactors. Chem Eng Sci 55: 2257-2263.
11. Merchuk JC, Contreras A, Garcia F, Molina E (1998) Studies of mixing in a concentric tube airlift bioreactor with different spargers. Chem Eng Sci 53: 709-719.
12. Snape JB, Zahradnik J, Fialova M, Thomas NH (1995) Liquid-phase properties and sparger design effects in an external-loop airlift reactor. Chem Eng Sci 50: 3175-3188.
13. Luo L, Liu F, Xu Y, Yuan J (2011) Hydrodynamics and mass transfer characteristics in an internal loop airlift reactor with different spargers. Chem Eng J 175: 494-504.
14. Chun S, Ming S, Farui H, Yingchun D (2005) Effect of Draft- Tube Structure on Gas-Liquid Flow in Airlift Loop Reactor. Petrochemical Technology 34: 959-964.